

Decondensation in non-equilibrium photonic condensates: when less is more

Henry J. Hesten, Robert A. Nyman,* and Florian Mintert

*Quantum Optics and Laser Science group, Blackett Laboratory,
Imperial College London, Prince Consort Road, SW7 2BW, United Kingdom*

(Dated: December 14, 2024)

We investigate the steady state of a system of photons in a pumped dye-filled microcavity. By varying pump and thermalization the system can be tuned between Bose-Einstein condensation, multimode condensation, and lasing. We present a rich non-equilibrium phase diagram which exhibits transitions between these phases, including decondensation under conditions that would typically favor condensation.

Phase transitions in systems governed by quantum statistics at thermal equilibrium have been investigated intensely. Canonical examples of these transitions are the formation of Cooper pairs in the superconductivity transition [1], or the transition of a thermal cloud of bosonic atoms to a Bose-Einstein (BEC) condensate as temperature decreases [2, 3]. The study of non-equilibrium phase transitions has spanned many disciplines from *classical* physics to social sciences [4], and explained many phenomena, such as trends in society [5], or traffic jams [6]. Only recently has attention turned to non-equilibrium phase transitions in *quantum* systems. For example the condensation of polaritons in semiconductor [7–9] or organic [10, 11] solids has been observed outside thermal equilibrium. Driven-dissipative many-particle quantum systems show intricate phase diagrams [12, 13], and bistability phenomena giving rise to coexisting phases have also been observed [14, 15].

Our system of study is a gas of photons confined in a dye-filled microcavity which, when the dye is pumped, can be made to thermalise and Bose-Einstein condense [16, 17]. Thermalization comes about because of the re-absorption of light by the dye [18], but since spontaneous emission limits spatial re-distribution of inhomogeneous pump light [19, 20] thermal equilibrium is always imperfect. If the cavity is far detuned from the dye molecular resonance, re-absorption is much slower than cavity loss and thermalization breaks down completely [21, 22].

Thermal-equilibrium theory predicts Bose-Einstein condensation, *i.e.* condensation in the lowest-energy mode. Multimode condensation [20, 23] is thus a clear signature of non-equilibrium behaviour, and extrapolating from prior experiments on non-equilibrium phase transitions [13, 15], one would expect that condensation is always favored by an increase in the pump rate [7, 16] and a decrease in thermalization rate. Whereas this is true at equilibrium and at low pump rates, we also find the opposite behaviour in the regime far out of equilibrium. That is, modes with condensed photons can

lose their macroscopic occupation as the pump rate is increased, which is similar to decreasing entropy as temperature increases, or negative heat capacities [24]. This gives rise to a highly complex dependence of the steady state on properties like pump rate, geometry, and the time-scale of thermalization. Based on numerical solutions of a microscopic model [21] we predict the dependence of multimode condensation on such properties. Despite the non-linear nature of the system we find some analytic laws characterising the condensation.

We study an externally pumped, dye-filled harmonic cavity. Since only one longitudinal mode is sufficiently close to resonance with the dye molecules, the cavity can be reduced to a two-dimensional model with transverse modes labeled by $m = [m_x, m_y]$. Taking into account loss through the mirrors and spontaneous emission from dye molecules into modes that are not confined within the cavity results in the well-established equation of motion [20]

$$\frac{dn_m}{dt} = -\kappa n_m + \rho \Gamma_{\downarrow}^{(m)} f_m (n_m + 1) + \rho \Gamma_{\uparrow}^{(m)} (f_m - 1) n_m, \quad (1)$$

for the average occupation n_m of mode m , where κ is the cavity decay constant, $\Gamma_{\uparrow}^{(m)}$ and $\Gamma_{\downarrow}^{(m)}$ are respectively the rates of absorption from and emission into mode m ; f_m is the fraction of excited molecules interacting with mode m , and it is given in terms of the fraction $f(\mathbf{r})$ of molecules at point \mathbf{r} which are excited and the mode-profile $\psi_m(\mathbf{r})$ via the relation $f_m = \int d^2\mathbf{r} f(\mathbf{r}) |\psi_m(\mathbf{r})|^2$. The dynamics of the excited-state population is governed by

$$\frac{\partial f(\mathbf{r})}{\partial t} = -\Gamma_{\downarrow}^{tot}(\mathbf{r}) f(\mathbf{r}) + \Gamma_{\uparrow}^{tot}(\mathbf{r}) (1 - f(\mathbf{r})), \quad (2)$$

in terms of the rates of total absorption and emission, $\Gamma_{\downarrow}^{tot}(\mathbf{r})$ and $\Gamma_{\uparrow}^{tot}(\mathbf{r})$, which depend on the mode occupations via

$$\Gamma_k^{tot}(\mathbf{r}) = \Gamma_k(\mathbf{r}) + \sum_m |\psi_m(\mathbf{r})|^2 \Gamma_k^{(m)} (n_m + \delta_{k\downarrow}) \quad (3)$$

with $k = \uparrow, \downarrow$ and $\delta_{\uparrow\downarrow} = 1 - \delta_{\downarrow\uparrow} = 0$. The steady

* r.nyman@imperial.ac.uk

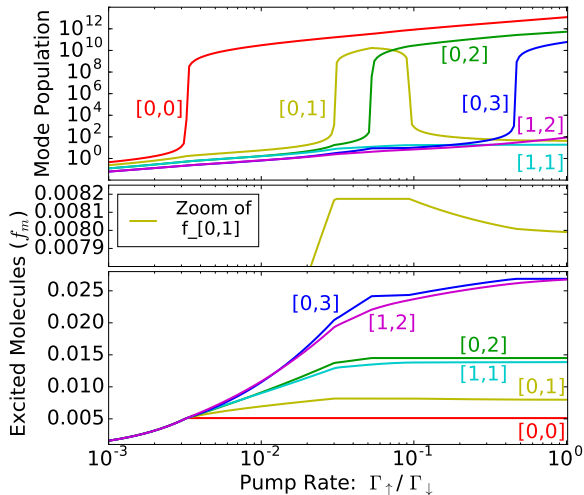


FIG. 1. The upper panel depicts the mode populations n_m as functions of pump rate for a constant thermalization rate $\gamma = 1.8$. One can clearly see how mode $[0, 1]$ condenses and then de-condenses with increasing pump rate. The lower panel depicts the fraction of excited molecules f_m accessible to any mode, and substantiates that the decondensation of mode $[0, 1]$ is congruent with decrease of $f_{[0,1]}$ as highlighted in the central panel, which is a magnification of the lower panel.

state ($\dot{f}_m = 0$) solution of Eq. (2) is obtained for

$$f_m^{(s)} = \int d^2\mathbf{r} |\psi_m(\mathbf{r})|^2 \frac{\Gamma_{\uparrow}^{tot}(\mathbf{r})}{\Gamma_{\uparrow}^{tot}(\mathbf{r}) + \Gamma_{\downarrow}^{tot}(\mathbf{r})}. \quad (4)$$

The steady-state solution of Eq. (1), together with Eq. (4), can be found with algebraic root finding routines, and we verified explicitly that the obtained solutions coincide with the solutions obtained by propagation until a stationary state is reached.

We choose parameter values appropriate to real experiments, but specify all values in units of cavity decay κ (which for typical experiments is of the order of $10^{12}/\text{s}$) and harmonic oscillator length L (the mean spatial extent of the lowest cavity mode). The shape of absorption and emission profiles $\Gamma_{\uparrow/\downarrow}^{(m)}$ for the individual modes are extracted from experimental data [19] and their peaks are set to $1.2 \times 10^{-9} \kappa$ (see appendix A). We consider a slightly anisotropic cavity with mode spacings $\omega_x = \omega_y/1.01 = 3 \times 10^4 \kappa$, and a detuning between the molecular resonance frequency and the lowest cavity eigenfrequency ranging from $-3.5 \times 10^5 \kappa$ to $-1.89 \times 10^5 \kappa$. The pump of the molecules of areal density $\rho = 10^{12}/L^2$ has a Gaussian profile with width $20L$, and the decay rate Γ_{\downarrow} of excited molecules is set to $\Gamma_{\downarrow} = \kappa/4$. The anisotropy of the cavity is chosen in order to avoid degeneracies, but it is sufficiently small so that mode pairs $[a, b]$ and $[b, a]$ behave almost identically, and their condensation thresholds are hardly distin-

guishable. We will therefore only discuss modes $[a, b]$ with $a > b$. In order to arrive at a finite-dimensional problem, we consider cavity modes with $m_x + m_y \leq 6$ only.

As the thermalization process occurs when excitations are exchanged between cavity modes and dye molecules, we compare the rate of absorption $\rho\Gamma_{\uparrow}^{(m)}$ to the rate of loss κ and define the thermalization coefficient $\gamma = \rho\Gamma_{\uparrow}^{[0,0]}/\kappa$. When γ is greater than one, the photons are more likely than not to scatter from a molecule before leaving the cavity, and are therefore thermalized. When γ is less than one, most photons are lost from the cavity before being absorbed and they do not thermalize.

Fig. 1 (top panel) depicts mode occupations as functions of pump rate, and one can see step-like increases and decreases of the populations, *i.e.* condensation and decondensation of individual modes at specific values of pump rate. The BEC phase is defined by condensation in the lowest cavity mode only, whereas a multimode-condensate contains additional condensed modes. Any phase with one or more condensed modes, but an uncondensed ground mode is considered a laser, and any phase without any condensed modes will be called un-condensed.

Defining the boundary between such phases can be done unambiguously in the thermodynamic limit, but it poses an intricate problem in systems of finite size. Since we observe large increases in the population of a single mode under small changes of driving conditions (as depicted in Fig. 1 (top panel)) we employ this as an indicator of condensation threshold [7, 23]. Quantitatively, we define the threshold of condensation (decondensation) as an increase (decrease) in population greater than 3 orders of magnitude over an increase in pump rate of 10%, but due to the sharp nature of all observed transitions, the identification of threshold is largely independent of the explicitly chosen numerical values.

For appropriate parameters the simulation qualitatively reproduces the single-mode condensation behaviour seen in experiments [16, 19]. In accordance with more recent experimental observations [23], multimode condensation is found for strong pumping and slow thermalization as shown in Fig. 2.

With this characterization at hand, we can now show how varying the thermalization coefficient γ and pump rate Γ_{\uparrow} leads to a range of steady-state phase transitions, including multimode condensation and even decondensation. Fig. 2 shows the phase of the system as the pump rate and thermalization coefficient are varied. At lower pump rates the system is in the un-condensed phase, with no condensed modes. At large thermalization coefficient and pump rate the system is in the BEC phase. As the thermalization coefficient is decreased from here, the system passes through

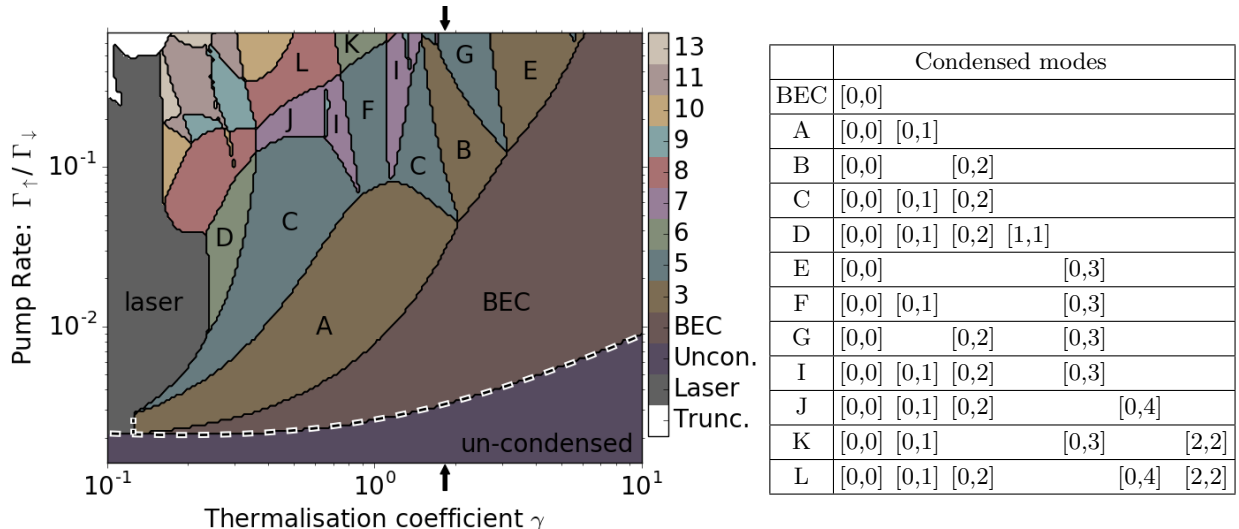


FIG. 2. Phase diagram of the photon gas as function of pump rate Γ_{\uparrow} and thermalization coefficient γ . Different colors indicate the number of condensed modes with the sole exceptions of ‘laser’, which indicates condensed phases of the system without condensation in the ground mode, and ‘truncated’ indicating potential truncation errors. Capital letters indicate which modes are condensed in a given region; narrow areas in which only one of modes $[a, b]$ and $[b, a]$ are condensed are treated as if both modes were condensed in order to avoid too detailed structures. The analytic prediction (Eq. (11)) for condensation threshold (dashed line) coincides very accurately with the numerically obtained threshold. The trend that strong pumping and weak thermalization favors condensation is observed for the onset of Bose-Einstein- and multi mode condensation, but in the regime of multi-mode condensation the behaviour becomes more complicated and decondensation can be induced through an increase in pump rate Γ_{\uparrow} as depicted in more detail (for $\gamma = 1.8$, indicated by bold arrows) in Fig.1, or a decrease in thermalization coefficient γ .

various multimode states, until the ground mode is no longer condensed and the system becomes a laser, which confirms that Bose-Einstein condensation is a thermal phenomenon, whereas lasing is not.

Given the system’s intrinsically non-linear character it is difficult to make analytic predictions about multimode condensation or decondensation, but we can predict the onset of single-mode condensation rather accurately assuming a spatially homogeneous system (see appendix C for a more detailed derivation). Below condensation threshold, the term proportional to n_m in Eq. (3) can be neglected, such that the mode occupation in the stationary state following Eqs. (1) and (4) reads

$$n_m^{(s)} = \frac{\Gamma_{\downarrow}^{(m)} \Gamma_{\uparrow}}{\frac{\kappa}{\rho} (\Gamma_{\uparrow} + \Gamma_{\downarrow}) + \Gamma_{\uparrow}^{(m)} \Gamma_{\downarrow} - \Gamma_{\downarrow}^{(m)} \Gamma_{\uparrow}}.$$

Condensation of mode m is expected to occur if the denominator vanishes, which happens for

$$\frac{\Gamma_{\uparrow}}{\Gamma_{\downarrow}} = \frac{\rho \Gamma_{\uparrow}^{(m)} + \kappa}{\rho \Gamma_{\uparrow}^{(m)} e^{-\beta \delta_m} - \kappa}, \quad (5)$$

where we have used the Kennard-Stepanov/McCumber relation [25–27] $\Gamma_{\downarrow}^{(m)} = \Gamma_{\uparrow}^{(m)} e^{-\beta \delta_m}$ in terms of the inverse temperature $\beta = 1/(k_B T)$, and δ_m is the detuning of mode m from the zero-phonon line. For slow

decay from the cavity $\kappa \ll \rho \Gamma_{\uparrow}^{(m)}$ this reduces to the approximation $\Gamma_{\uparrow}^{(m)}/\Gamma_{\downarrow} \approx e^{\beta \delta_m}$ [21].

The thermalization coefficient γ is directly related to the detuning, but since this relation depends on the absorption spectrum of the molecules there is no simple analytical form for it. Nevertheless, since γ is the more informative quantity, we will mostly refer to thermalization in the following. The increase of the threshold pump rate with γ as predicted by Eq.(11) is depicted in Fig. 2 with a white dashed line, and it fits the numerically obtained threshold extremely well. The vertical dashed line indicates the value of γ above which Eq.(11) predicts that the mode at condensation threshold will be the lowest energy mode. This prediction exactly matches the transition from BEC to lasing when close to threshold.

The qualitative trend that condensation can be induced by increasing pump rate Γ_{\uparrow} or decreasing thermalization rate γ is also observable for multimode condensation in Fig. 2, but the exact instances of condensation and decondensation are substantially more complicated than the simple law of Eq. (11). An example of condensation and decondensation is depicted in Fig. 1 (top panel) where the populations of the lowest modes are shown as functions of pump rate for $\gamma = 1.8$. There is a step-like increase in the population of the lowest mode $m = [0, 0]$ around $\Gamma_{\uparrow}/\Gamma_{\downarrow} \simeq 0.003$ followed by the condensation of modes $[0, 1]$, and

subsequently [0, 2]. One can also see that the population of mode [0, 1] decreases as mode [0, 2] condenses, and that mode [0, 1] de-condenses around $\Gamma_{\uparrow}/\Gamma_{\downarrow} \simeq 0.09$. In general, one would expect condensation to be favored by a strong pump which takes the system out of equilibrium, but decondensation with increasing pump rate seems highly counter-intuitive.

Nevertheless, we can develop an understanding in terms of the decomposition of the total pump rate into individual contributions given in Eq. (3). For low populations n_m of all modes, the total rates of absorption/emission can be well approximated by pumping and loss, *i.e.* Eq. (3) reduces to $\Gamma_{\uparrow/\downarrow}^{tot}(\mathbf{r}) \simeq \Gamma_{\uparrow/\downarrow}(\mathbf{r})$, so that the pumping of dye molecules (Eq. (2)) is proportional to the external pumping. In the case of strongly occupied modes, on the other hand, the approximation $\Gamma_{\uparrow/\downarrow}^{tot}(\mathbf{r}) \simeq \sum_m |\psi_m(\mathbf{r})|^2 \Gamma_{\uparrow/\downarrow}^m n_m$ in terms of the rates $\Gamma_{\uparrow/\downarrow}^m n_m$ of stimulated absorption and emission holds, and the proportion of excited dye molecules is largely independent of external pumping but depends mostly on the interaction with the condensed mode or modes. Molecules in spatial domains where $|\psi_m(\mathbf{r})|^2 \Gamma_{\uparrow/\downarrow}^m n_m$ is sufficiently large to satisfy this regime are thus *clamped* to mode m .

As pumping is increased the fraction of excited clamped molecules decreases, but the excitation of un-clamped molecules is growing, and, in particular, un-condensed modes thus experience a growing reservoir of excitations that can help them to gain enough population to condense. As a mode condenses, however, it also starts to clamp dye molecules and the number of molecules clamped to this mode grows with increasing population n_m . This mode thus enters a competition for access to excitations with the other modes, and potentially reduces the access for other modes, which can result in their decondensation.

This effect can be explicitly seen in the fraction of excited molecules f_m accessible to mode m as shown in Fig. 1 (center and bottom panel). The center panel magnifies $f_{[0,1]}$ and shows that $f_{[0,1]}$ decreases with increasing pump rate after the condensation of mode [0, 2], despite the general (and expected) trend that f_m grows with increasing pump rate.

Quite strikingly, the decrease in accessible excited dye molecules required for decondensation is rather minute and visible only in the magnified panel. Nevertheless, it has an extremely significant impact on the condensation behavior, and the impact of reduced access to excited molecules becomes increasingly consequential as the number of condensed modes grows. Fig. 2 depicts several instances where small changes in pumping of thermalization result in a substantial redistribution of populations between the modes, and multiple triple- and quadruple-points.

Current experiments are performed for γ rang-

ing between 0.2 and 5 and pump rates reach rates ten times the threshold value [23]. Exploring the upper half of the phase diagram presented in Fig. 2, requires substantially stronger pumping than currently realised. Since pulsed lasers can achieve peak pump rates three orders of magnitude higher than CW lasers, with pulse durations longer than the time taken to reach steady state, this seems a perfectly viable option. The model we have used is applicable to a wide range of systems which need only satisfy a few criteria: an optical environment with a well-defined ground state; a fluorescent gain medium which meets the Kennard-Stepanov/McCumber relation and re-scattering of light faster than loss for thermalisation. We thus expect that the crossover from thermal equilibrium to lasing via multimode condensation will be observable in semiconductors in photonic crystal resonators [28], and trapped exciton-polariton or organic-polariton condensates, as well as dye-microcavity photon condensates.

The rich interplay between the different modes observed in Fig. 2 also offers great opportunities for the creation of tailored states of light [29], since the mode structure can easily be influenced through the shape of the cavity [30] and the spatial pump profile can be varied. Since fluctuations are most relevant near phase transitions, we expect this rich phase diagram to be a fruitful tool in the search for unusual quantum correlations.

Appendices

In the appendix we discuss the absorption and emission spectra used in the simulation, followed by a justification for our choice of threshold condition. We present a fuller analytic derivation of the boundary between the un-condensed and condensed phases. Then we show how a variation of pump profile induces multimode condensation and decondensation, similarly to the variation of thermalization that is discussed in the main paper.

A. ABSORPTION AND EMISSION SPECTRA

All parameter values used for simulations match current photon BEC experiments [19]. The only difference between simulations and typical experiment values is in the mode spacing. We use a mode spacing of 30 Trad/s (*i.e.* $30/(2\pi)10^{12}$ Hz) as this enables us to consider a system with few occupied modes, keeping it computationally tractable. Spacings in current experiments are a factor of 10 smaller, but there is no fundamental difficulty in experiments with larger spacings.

The absorption (emission) of light from (into) a cavity mode with detuning δ by molecules is derived from experimental data, shown in Fig. 3.

The blue crosses indicate experimental data with a peak value of $1.2/s$. In our simulations we use $1.2 \times 10^{-9}\kappa$ as peak value, and we use the fitted dependence satisfying the Kennard-Stepanov/McCumber relation, depicted in black.

The cavity modes have detunings of $\delta = \delta_{[0,0]} + m_x\omega_x + m_y\omega_y$ with $\omega_x = 30$ Trad/s and $\omega_y = 30.3$ Trad/s, and m_x and m_y are the integers labeling each mode; $\delta_{[0,0]}$ is the detuning of the lowest mode from the molecular splitting and ranges from -350 Trad/s to -180 Trad/s.

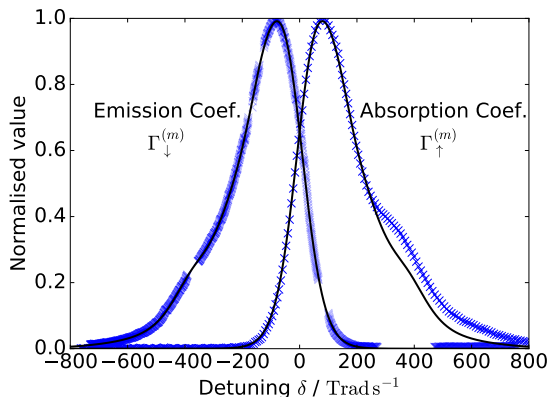


FIG. 3. (Crosses) The experimental absorption and emission data. (Solid) The fits to this data.

B. THRESHOLD

The threshold condition used in our simulations is an increase in the population of a mode greater than 3 orders of magnitude over an increase in pump rate of 10%. Here we justify our claim that the precise values used do not significantly change the phase diagram by presenting the large difference in mode population between the condensed and un-condensed modes.

Fig. 4 depicts a histogram for the occurrence of given mode populations. The data depicted in green corresponds to all modes considered un-condensed in the phase diagram depicted in Fig. 2 of the main article, and data depicted in blue corresponds to modes categorized as condensed. As one can see, each condensed mode has a population larger than $10^{5.8}$ and each un-condensed mode has a population smaller than $10^{5.8}$, with the exception of 8 mis-categorized points with a population of about 10^5 . Inspection of these points reveals that they are part way through a condensation or de-condensation, and therefore constitute the shifting of a phase boundary by only a single sample. Changing the threshold condition to a change in population $10^{3.4}$ instead of 10^3 would result in perfect agreement between the threshold condition and the bi-modal distribution depicted in Fig. 4.

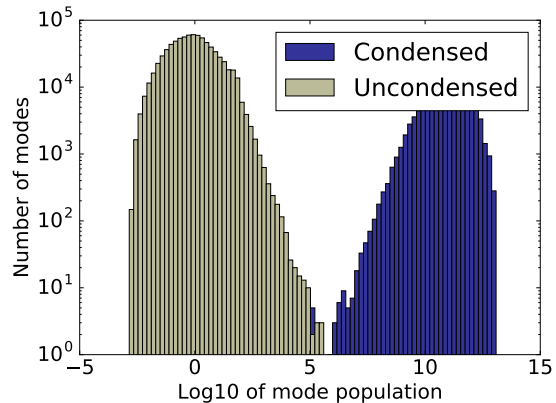


FIG. 4. Histogram of the mode populations for all modes and all parameter values depicted in the phase diagram (Fig. 2) of the main article.

C. ANALYTIC PHASE BOUNDARIES

Here we derive analytical expressions for the boundary between the un-condensed and the BEC phase, the un-condensed and laser phase, and the boundary between the BEC and laser phases just above condensation threshold.

Below condensation threshold the mode populations satisfy $n_m \ll 1$, and their equation of motion Eq. (1) can be approximated as

$$\begin{aligned} \frac{dn_m}{dt} &= -\kappa n_m + \rho \Gamma_{\downarrow}^{(m)} f_m(n_m + 1) \\ &\quad + \rho \Gamma_{\uparrow}^{(m)} (f_m - 1) n_m \\ &\simeq -\kappa n_m + \rho \Gamma_{\downarrow}^{(m)} f_m. \end{aligned} \quad (6)$$

Similarly, the relation between the different pump rates (Eq.(3)) reduces to

$$\begin{aligned} \Gamma_{\uparrow}^{tot}(\mathbf{r}) &= \Gamma_{\uparrow}(\mathbf{r}) + \sum_m |\psi_m(\mathbf{r})|^2 \Gamma_{\uparrow}^{(m)} (n_m + \delta_{k\downarrow}) \\ &\simeq \Gamma_{\uparrow}(\mathbf{r}) \\ \Gamma_{\downarrow}^{tot}(\mathbf{r}) &= \Gamma_{\downarrow}(\mathbf{r}) + \sum_m |\psi_m(\mathbf{r})|^2 \Gamma_{\downarrow}^{(m)} (n_m + \delta_{k\downarrow}) \\ &= \Gamma_{\downarrow}(\mathbf{r}) + \sum_m |\psi_m(\mathbf{r})|^2 \Gamma_{\downarrow}^{(m)}. \end{aligned} \quad (7)$$

In the case of spatially homogeneous pumping, the absorption and emission rates $\Gamma_{\uparrow/\downarrow}^{tot}(r)$ can be approximated as spatially independent, and the excited state populations $f_m^{(s)}$ (Eq. (4)) in the steady state reduce to

$$f_m^{(s)} \simeq \frac{\Gamma_{\uparrow}^{tot}}{\Gamma_{\uparrow}^{tot} + \Gamma_{\downarrow}^{tot}}. \quad (8)$$

Eqs. (6) and (8) together predict the occupation

$$n_m = \frac{\Gamma_{\downarrow}^{(m)} \Gamma_{\uparrow}}{\frac{\kappa}{\rho} (\Gamma_{\uparrow} + \Gamma_{\downarrow}) + \Gamma_{\uparrow}^{(m)} \Gamma_{\downarrow} - \Gamma_{\downarrow}^{(m)} \Gamma_{\uparrow}} \quad (9)$$

of mode m . With the Kennard-Stepanov/McCumber relation $\Gamma_{\downarrow}^{(m)} = \Gamma_{\uparrow}^{(m)} e^{-\beta\delta_m}$, this reduces to

$$n_m = \frac{\Gamma_{\uparrow}}{\frac{\kappa}{\rho} \frac{\Gamma_{\uparrow} + \Gamma_{\downarrow}}{\Gamma_{\downarrow}^{(m)}} + e^{\beta\delta_m} \Gamma_{\downarrow} - \Gamma_{\uparrow}} \quad (10)$$

Condensation threshold is expected around the divergence of the denominator in Eq. (10), *i.e.* for

$$\frac{\Gamma_{\uparrow}}{\Gamma_{\downarrow}} = \frac{\rho\Gamma_{\uparrow}^{(m)} + \kappa}{\rho\Gamma_{\downarrow}^{(m)} e^{-\beta\delta_m} - \kappa}. \quad (11)$$

Given the assumption $n_m \ll 1$, Eq.(11) applies to the first condensation threshold only, *i.e.* it predicts the condensation of the mode m with the lowest threshold pump power. If this is the lowest mode, then Eq.(11) describes the threshold of Bose-Einstein condensation; otherwise it predicts the onset of lasing.

D. DEPENDENCE ON PUMP SPOT SIZE

A natural parameter which is easily varied in an experiment is the width of the pump profile. In the main paper, we consider an essentially homogeneous pump profile. Narrow pump profiles have already been used to experimentally achieve multimode condensation, and they do so at lower total pump powers [23] since a larger fraction of the

power is concentrated on the central, condensed modes. We therefore also investigated the dependence of the photon gas on the pump width, with a Gaussian pump profile centered around the center of the cavity.

If the width of the pump profile is narrower than the spatial extent of the lowest cavity mode, then pumping is mostly restricted to this mode. The majority of the pumped dye molecules are therefore clamped by this mode, which prevents multimode condensation. One therefore obtains single-mode BEC even for very strong pumping.

With increasing pump width excited modes also experience pumping, and sufficiently strong pumping results in multimode condensation. As the pump spot size is increased further, the pump power is distributed over more modes, and some modes lose their macroscopic occupation. There is thus an optimal pump spot size at which multimode condensation can be achieved with minimal pump power. We found this size to be about 1.4 times larger than the mean spatial extent of the ground-state wavefunction.

We acknowledge fruitful discussions with David Newman, Peter Kirton and Jonathan Keeling, and financial support from the UK EPSRC (via fellowship EP/J017027/1 and the Controlled Quantum Dynamics CDT EP/L016524/1), and the ERC (via ODYCQUENT grant). After publication the data underlying this article will be available at <http://doi.org/10.5281/zenodo.569817>

-
- [1] J. Bardeen, L. N. Cooper, and J. R. Schrieffer, Phys. Rev. **108**, 1175 (1957).
 - [2] M. Anderson, J. Ensher, M. Matthews, C. Wieman, and E. Cornell, Science **269**, 14 (1995).
 - [3] K. B. Davis, M.-O. Mewes, M. R. Andrews, N. Van Druten, D. Durfee, D. Kurn, and W. Ketterle, Phys. Rev. Lett. **75**, 3969 (1995).
 - [4] S. Lübeck, Int. J. Mod. Phys. **18**, 3977 (2004).
 - [5] W. Weidlich, Physics Reports **204**, 1 (1991).
 - [6] B. S. Kerner and H. Rehborn, Phys. Rev. Lett. **79**, 4030 (1997).
 - [7] J. Kasprzak, M. Richard, S. Kundermann, A. Baas, P. Jeambrun, J. Keeling, F. Marchetti, M. Szymańska, R. Andre, J. Staehli, *et al.*, Nature **443**, 409 (2006).
 - [8] H. Deng, D. Press, S. Götzinger, G. S. Solomon, R. Hey, K. H. Ploog, and Y. Yamamoto, Phys. Rev. Lett. **97**, 146402 (2006).
 - [9] R. Balili, V. Hartwell, D. Snoke, L. Pfeiffer, and K. West, Science **316**, 1007 (2007).
 - [10] J. D. Plumhof, T. Stöferle, L. Mai, U. Scherf, and R. F. Mahrt, Nat. Mater. **13**, (2014).
 - [11] K. Daskalakis, S. Maier, R. Murray, S. Kéna-Cohen, *et al.*, Nat. Mater. **13**, 271 (2014).
 - [12] A.-W. de Leeuw, O. Onishchenko, R. A. Duine, and H. T. C. Stoof, Phys. Rev. A **91**, 033609 (2015).
 - [13] M. Fitzpatrick, N. M. Sundaresan, A. C. Y. Li, J. Koch, and A. A. Houck, Phys. Rev. X **7**, 011016 (2017).
 - [14] D. Sarchi, I. Carusotto, M. Wouters, and V. Savona, Phys. Rev. B **77**, 125324 (2008).
 - [15] J. M. Fink, A. Dombi, A. Vukics, A. Wallraff, and P. Domokos, Phys. Rev. X **7**, 011012 (2017).
 - [16] J. Klaers, J. Schmitt, F. Vewinger, and M. Weitz, Nature **468**, 545 (2010).
 - [17] J. Klaers, F. Vewinger, and M. Weitz, Nat. Phys. **6**, 512 (2010).
 - [18] J. Schmitt, T. Damm, D. Dung, F. Vewinger, J. Klaers, and M. Weitz, Phys. Rev. A **92**, 011602 (2015).
 - [19] J. Marelic and R. Nyman, Phys. Rev. A **91**, 033813 (2015).
 - [20] J. Keeling and P. Kirton, Phys. Rev. A **93**, 013829 (2016).
 - [21] P. Kirton and J. Keeling, Phys. Rev. Lett. **111**, 100404 (2013).
 - [22] P. Kirton and J. Keeling, Phys. Rev. A **91**, 033826 (2015).
 - [23] J. Marelic, L. F. Zajiczek, H. J. Hesten, K. H. Leung, E. Y. X. Ong, F. Mintert, and R. A. Nyman, New J. Phys. **18**, 103012 (2016).

- [24] K. Michaelian and I. Santamaría-Holek, EPL (Europhysics Letters) **79**, 43001 (2007).
- [25] E. Kennard, Phys. Rev. **11**, 29 (1918).
- [26] B. Stepanov, Soviet Physics Doklady **2**, 81 (1957).
- [27] D. E. McCumber, Phys. Rev. **136**, A954 (1964).
- [28] A.-W. de Leeuw, E. C. I. van der Wurff, R. A. Duine, D. van Oosten, and H. T. C. Stoof, Phys. Rev. A **94**, 013615 (2016).
- [29] T. Hisch, M. Liertzer, D. Pogany, F. Mintert, and S. Rotter, Phys. Rev. Lett. **111**, 023902 (2013).
- [30] L. Flatten, A. Trichet, and J. Smith, Laser & Photonics Reviews **10**, 257 (2015).